PAPER

Check for updates

Sorting and decoration of semiconducting single-walled carbon nanotubes *via* the quaternization reaction†

Ying Luo,[a] Yuemaierjiang Maimaiti,[a] Xieraili Maimaitiyiming, [ORCID] *[a] Chuang Xie [ORCID] [b] and Tiezhu Pei[b]

A study for the selective separation and functionalization of alcohol-soluble semiconducting single-walled carbon nanotubes (sc-SWCNTs) is carried out by polymer main-chain engineering. Introducing tertiary amine groups endows the functionalized sc-SWCNTs with alcohol-soluble properties and introducing the pyrimidine rings allows to increase the selective purity of sc-SWCNTs. In this study, a series of poly [(9,9-dioctylfluorene)-2,7-(9,9-bis(3′-(N,N-dimethylamino)propyl)-fluorene]$_m$-*alt*-[2-methylpyrimidine-2,7-(9,9-dioctylfluorene)]$_n$ (PFPy) are used for the selective dispersion of semiconducting single-walled carbon nanotubes, where *n* and *m* are the composition ratio of the copolymer. When *m* = *n*, the effective isolation of sc-SWCNTs with purity greater than 99% is achieved. The alcohol-soluble sc-SWCNTs with a diameter in the range of 1.1–1.4 nm are obtained through designing reasonable molecular structure. Moreover, the particular preference of PFPy (*m* = *n*) for sc-SWCNTs was studied *via* density functional theory (DFT) calculations and it was proved to be a promising method for the separation and functionalization of sc-SWCNTs.

Introduction

Since the discovery of single-walled carbon nanotubes (SWCNTs) in 1991,[1] considerable efforts have been made to develop their flexible electronics,[2,3] and mechanical[4,5] and optoelectronic properties.[6–8] In the commercial syntheses, the produced raw SWCNTs are complex mixtures containing metallic and semiconducting nanotubes, and amorphous carbon and metal catalyst residues.[9–11] For many applications, such as thin film transistors (TFTs), integrated circuits and solar cells,[12,13] a higher sc-purity or sc-SWCNTs with minimal m-SWCNTs impurities are required.[14] Currently, numerous methods for separating sc- and m-SWCNTs have been reported, *e.g.*, density gradient ultracentrifugation,[15] DNA separation,[16] chromatography,[17] surfactant-assisted purification[18] and extraction using conjugated polymers (CPs).[19] Among these methods, the extraction with conjugated polymers has great potential for the development of sepratation sc-SWCNTs due to its low-cost, simple and extensible structure. In recent research,

researchers who committed to study carbon nanotubes have developed some selective and functionalized polymers to release sc-SWCNTs.[20–23] However, without ample attention has been employed the derivatized polymers that modified polymer/SWCNTs composite though functional reaction. The sc-SWCNTs selective separation is highly dependent on polymer structures and solvent properties, such as viscosity, polarity and density.[24,25] At present, most researches have concentrated on nonpolar solvents to obtain the pure sc-SWCNTs.[26–30] Of course, a few successful examples that were used to enrich the sc-SWCNTs using polar solvents, while amphiphilic/hydrophilic side chains were required for this polymer.[29,31]

In actual production, SWCNTs dispersed in organic solvents have caused a great harm to the surroundings and human body, while hydrophilic solvents have the opposite effect, such as water and alcohol solvents. Adronov *et al.* developed some reactive azido-based polyfluorenes,[32,33] which were unable to disperse the pure sc-SWCNTs or m-SWCNTs in D$_2$O. Also, these polyfluorenes were limited to a study in the laboratory due to the hazardous nature of the reaction process and inability to scale up. In addition, Malenfant *et al.* demonstrated that hydrophilic SWCNTs dispersions are suitable for ink formulation and high-performance printing thin-film transistor (TFT) fabrication since they possess the ideal rheological properties.[31,34]

Here, a route to functionalize and selectively separate alcohol-soluble sc-SWCNTs has been developed. The introduction of tertiary amine groups assists sc-SWCNTs to be dispersed in environmentally benign alcohol solvent, namely green solvent.

[a]Key Laboratory of Energy Materials Chemistry, Ministry of Education, Key Laboratory of Advanced Functional Materials, Autonomous Region, Institute of Applied Chemistry, College of Chemistry, Xinjiang University, Urumqi, 830046, Xinjiang, PR China. E-mail: 380731363@qq.com

[b]National Engineering Research Center of Industrial Crystallization Technology, School of Chemical Engineering and Technology, Tianjin University, Tianjin 300072, PR China

Also, the introduction of pyrimidine rings can improve the sorting of polymers for sc-SWCNTs. In series of poly[(9,9-dioctylfluorene)-2,7-(9,9-bis(3'-(N,N-dimethylamino)propyl)-fluorene)]$_m$-alt-[2-methylpyrimidine-2,7-(9,9-dioctylfluorene)]$_n$, the effective isolation of sc-SWCNTs with purity greater than 99% is obtained when $m = n$. The characteristic peaks of alcohol-soluble sc-SWCNTs are observed by UV-Vis-NIR absorption. Raman scattering shows that the electronic structure of the sc-SWCNTs is preserved after the quaternization reaction (QR). The density functional theory (DFT) calculations show that electron-rich conjugated polymers merely sort sc-SWCNTs, while the electron-poor counterparts sort m-SWCNTs.

Experimental

Materials

Bromoethane (analytical reagent) and dimethyl sulfoxide (DMSO) were purchased from Braunwell Technology Co, Ltd. Tetrahydrofuran (THF) (via refluxing at 60 °C to obtain THF), toluene (TL) and sodium dodecylbenzenesulfonate (SDBS) were obtained from J&K Scientific Co. Ltd., Beijing, China. Both THF and DMSO were gas blown with argon and then stored under argon atmosphere. Purified plasma nanotubes powder RN-220 (Batch # RN 31-54-220) was purchased from XFNANO Materials Tech Co. Ltd. and used without any further treatment.

Poly[(9,9-dioctylfluorene)-2,7-(9,9-bis(3'-(N,N-dimethylamino)propyl)-fluorene)]$_m$-alt-[2-methylpyrimidine-2,7-(9,9-dioctylfluorene)]$_n$ have been reported as sensors for detecting Al^{3+} in our laboratory (details of the synthesis method and characterization see ref. [35]). Here, they were applied to separate semiconducting single-walled carbon nanotubes. According to the various molar ratios of tertiary amine group, four poly[(9,9-dioctylfluorene)-2,7-(9,9-bis(3'-(N,N-dimethylamino)propyl)-fluorene)]$_m$-alt-[2-methylpyrimidine-2,7-(9,9-dioctylfluorene)]$_n$ were named PFA, PFPy-85, PFPy-50 and PFPy-15, respectively (ESI, Scheme S1†).

Characterization

Ultrasonication was done in a KQ5200B bath sonicator (Kunshan, Jiang Su, China). UV-Vis-NIR spectra were recorded by a Shimadzu UV-3600 spectrophotometer (Kyoto, Japan). Raman measurements were performed on a SENTERRA Raman spectrometer. A polytetrafluoroethylene (PTFE) filter (pore size 0.45 and 0.22 μm, Nylon 66) was used for filtration. Copolymers were optimized via density functional theory (DFT) geometry optimization through Gaussian 09W at the B3LYP level using the 6-31G (d,p) basis set.

Selective process of sc-SWCNTs with polymers

1.0 mg of four different polymers was dissolved in 3.0 ml of distilled toluene (TL) and filtered through 0.22 μm pore of nylon filters before adding 1.0 mg of raw single-walled carbon nanotubes (raw SWCNTs). The different polymer@SWCNTs mixtures were sonicated for 2 h in an ice bath (20 °C ± 5 °C). Also, these mixtures were centrifuged at 15 000 rpm for 30 min at 10 °C to

obtain a supernatant, which were used as the resulting polymer@SWCNTs dispersion to analyze.

Process of the polymer@SWCNTs dispersion film

5 mg of raw SWCNTs was sonicated in a sodium dodecylbenzenesulfonate (SDBS) solution for 30 min using a 200 W sonicator to compare with the polymer@SWCNTs dispersion sample. Also, the raw SWCNTs dispersion was dropped on silicon wafers for Raman scattering detection. The polymer@SWCNTs dispersions were filtered with 0.22 μm pore of nylon filters and washed several times with THF to remove the remaining polymer. Then, the SWCNTs filter membrane was ultrasonically dispersed in distilled dichloromethane and dropped on clean silicon wafers for Raman detection.

Results and discussion

Sorting sc-SWCNTs with polymers and discuss the mechanism

The absorption features of single-walled carbon nanotubes depend on their respective chiralities and diameters. The specific nanotubes exhibited the particular transition energies arising from the interband transitions of the van Hove singularities.[34] The UV-Vis-NIR spectroscopy generally is applied to identify the optical characteristics of carbon nanotubes.

Fig. 1a shows that absorption spectra of SWCNTs that were extracted separately using different polymers at the polymer/SWCNTs mass ratio of 1 : 1. The absorbance features with SWCNTs can be grouped into four bands in the observed ranges: M11: 600–750 nm, S33: 440–600 nm, S22: 800–1150 nm
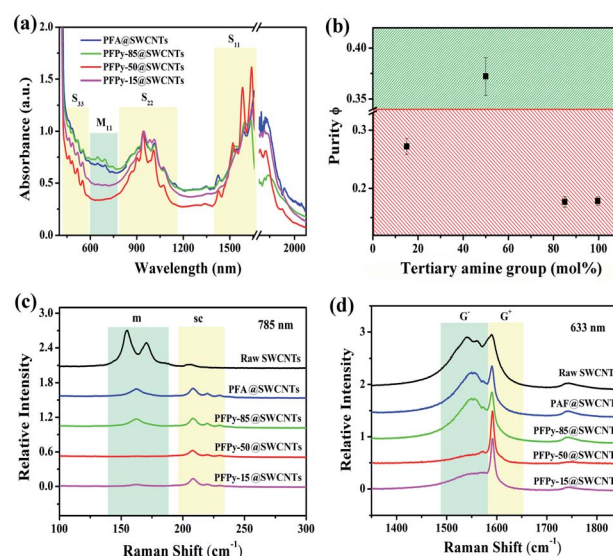

Fig. 1 (a) UV-Vis-NIR absorption spectra collected from samples that had PFA, PFPy-85, PFPy-50 and PFPy-15. The spectra normalized to the peak at 939 nm. (b) sc-SWCNTs purity of polymers with different proportions of tertiary amines that had polymers: SWCNTs ratio of 1 : 1. Raman scattering spectra of the polymer@SWCNTs complex obtained with polymers at (c) 785 nm and (d) 633 nm (all Raman spectra normalized to the G-band at approximately 1590 cm^{-1}).

and S11: 1400–1900 nm.[36] The last three bands were due to the optical characteristics from the valence band to conduction band with semiconducting SWCNTs. The strong dispersion ability of SWCNTs was displayed with four kinds of polyfluorenes. As the pyrimidine rings were continuously increased from PFA to PFPy-50, the m-SWCNTs were decreased regularly in the M11 region. The highest dispersion concentration of sc-SWCNTs ($\approx$ 1600 nm) and the deep "valley" in the M11 region were observed when $n = m$ (PFPy-50). The above-mentioned results showed that PFPy-50 sorted the high selectivity towards sc-SWCNTs. The relative remaining amount of m-SWCNTs in the dispersed samples can be confirmed by the absorption peak ratios of ϕ (sc-purity), both the first interband transition of m-SWCNTs and the second interband transition of sc-SWCNTs. The sc-purity of separation with a series of polymers of Fig. 1a corresponded to Fig. 1b. Among them, the sc-purity was selected by PFPy-50 greater than 0.33, which indicated that the content of sc-SWCNTs was over 99% in the sample.[31]

The electron-rich structures were conducive to separate sc-SWCNTs because of their strong effects of electron accumulation. The electron-rich pyrimidine rings, having typical structures, have been reported for selecting sc-SWCNTs.[23,28] The PFA structural unit also observed the electron-rich structure by DFT calculations (ESI, Fig. S2†). The PFA fragment was optimized in the solvent environment of toluene, and it showed 110.55° with the C–N–C angle of the tertiary amino groups. The intermolecular π–π stacking between polymers and sc-SWCNTs was hindered due to the large van der Waals radius around tertiary amine groups.[37,38] Therefore, augmented tertiary amino groups on the polymer were not conducive to enrich sc-SWCNTs. By increasing continually the pyrimidine rings to 85% while reducing the tertiary amine groups to 15% (PFPy-15), the characteristic peaks of m-SWCNTs were observed in the absorption band. Numerous polyfluorene were applied to various sensors because of their strong intermolecular π–π interactions.[39–41] The selectivity of the CP-SWCNTs interaction is influenced by the electronic nature of the CP backbone. Excessive pyrimidine rings may result from the unstable delocalized π-bonding in the conjugated systems of [[(9,9-dioctylfluorene)2,7-(9,9-bis(3′-(N,N-dimethylamino)propyl)-fluorene)]], which leads to the metallic nanotubes with more polar charge transfer that tend to be unavailable to aggregate and form sediment after centrifugation in toluene. Hence, a few m-SWCNTs were left in the supernatant. This observation showed the greater benefits to select sc-SWCNTs using the polymer with the equal amount of the tertiary amino groups and pyrimidine rings.

Numerous studies revealed the m- and sc-SWCNTs of C–C vibration behaviors by Raman scattering.[33,42,43] The in-plane stretching vibrations of sp^2 hybrid C atoms on carbon tubes are reflected at different excitation wavelengths. The strong peaks of radial breathing modes (RBM) with metallic SWCNTs were observed in the raw SWCNTs (Fig. 1c) under the 785 nm excitation. However, the RBM peaks almost disappeared after separation by PFA, PFPy-85 and PFPy-15. In particular, a flat line of PFPy-50@SWCNTs appeared in the metallic region, which indicated a high separation *via* PFPy-50. Fig. 1d shows G-mode

at the 633 nm excitation wavelength. The intensity of the G$^-$ peaks of metallic SWCNTs at 1480–1580 cm^{-1} decreased regularly, while that of the G$^+$ peaks of semiconducting carbon nanotubes nearly maintained at 1600 cm^{-1}, which indicated that there are no metallic carbon tubes in PFPy-50@SWCNTs dispersions after sorting PFPy-50. These results are completely consistent with the characterization results of UV-Vis-NIR spectroscopy.

To determine whether the functional reaction matters, we prepared the copolymer PFPy-50-Br* bromoethane. Also, the copolymer was used for dispersing raw SWCNTs in MeOH as a sample of PFPy-50-Br*@SWCNTs (see ESI for details†). Fig. 2a shows the UV-Vis-NIR spectra of PFPy-50-Br*@SWCNTs complexes. The strong peaks of the m-SWCNTs (green region) were observed. This result showed that PFPy-50-Br* had a good stripped efficacy instead of ability for sorting SWCNTs.

Prior to PFPy-50@SWCNTs functional complexation, we used the Gaussian 09W software to study the electronic performance of the copolymer unit for PFPy-50 and PFPy-50-Br* by density functional theory (DFT).[44,45] To reduce the calculated complexity and time, electronic analyses were performed to the polyfluorene that the octyl chain substituted with the methyl group. The DFT calculations suggested that the electronic landscape of the polymer backbones were altered drastically after the quaternization reaction.

Fig. 2b shows that the conjugated PFPy-50 was electron-rich, whereas the PFPy-50-Br* was a relatively electron-poor system. Additionally, PFPy-50 (2.4 Debye) was a nonpolar polymer and had a dielectric constant similar to that of toluene (polarity index values are taken from http://macro.lsu.edu/howto/solvents/Polarityindex.htm), which tends to form bundles with metallic SWCNTs in a given stable solvent,[46] thereby resulting in a higher selectivity towards sc-SWCNTs. The functional reaction of PFPy-50@SWCNTs, such as transformed from toluene to methanol, indicated the significant reduction of pollution to the environment. Also, the method that enriches sc-SWCNTs in alcohol was no longer hindered using the electron-poor polymer structures.

The polymer/SWCNTs ratio was another crucial factor that affected the selectivity of sc-SWCNTs. Fig. S3a† displays the concentrations of SWCNTs dispersions using PFPy-50 under numerous polymer/SWCNTs ratios. As the amount of PFPy-50 increased, the concentration of SWCNTs also increased gradually until the emergence of metallic carbon nanotubes. For PFPy-50, the optimal ratio (0.5/1) of polymer/SWCNTs exhibited high sc-purity ($\phi = 0.383$) (ESI, Fig. S3b†).

Functionalization of polyfluorene@sc-SWCNTs

Based on the consideration of dispersion ability and purity, an optimal ratio of PFPy-50/SWCNTs was expanded to 2/4 (ESI, Fig. S4†) for further studying functional reaction. Fig. S5† shows that the detailed procedures of the PFPy-50-Br@SWCNTs complex were prepared by the quaternization reaction (QR). Fig. 3 shows the process diagram of the separation and functionalization of sc-SWCNTs by copolymer PFPy-50. UV-Vis-NIR spectra and Raman scattering were recorded to characterize
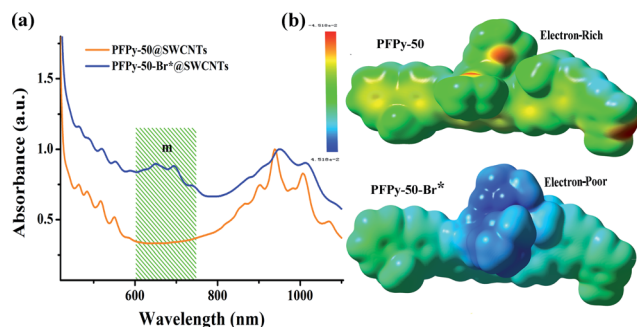
Fig. 2 (a) UV-Vis-IR spectra of PFPy-50@SWCNTs (orange line) dispersion and direct synthesis PFPy-50-Br*@SWCNTs (blue line) dispersion. (b) Electron-density maps of polymers for PFPy-50 and PFPy-50-Br* (red denotes electron-rich regions, green indicates less electron-rich areas, and blue denotes electron-poor regions).
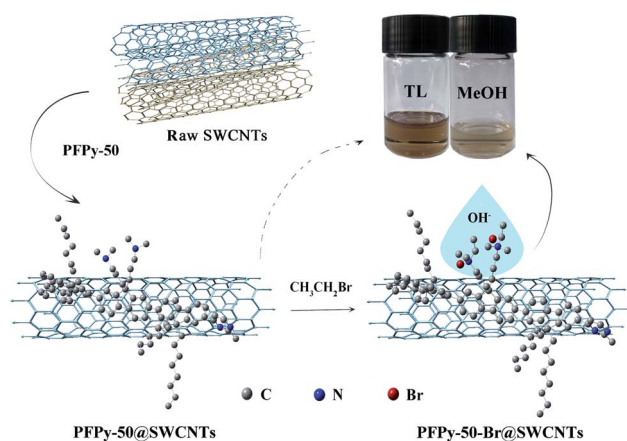

Fig. 3 Process diagram of sorting sc-SWCNTs and functionalization PFPy-50@SWCNTs. Also, the physical picture of the PFPy-50@SWCNTs dispersion with pre-QR and post-QR in TL and MeOH solvent, respectively.

the complex before and after QR. Compared with the PFPy-50@SWCNTs complex before QR (see ESI for detailed steps†), the PFPy-50-Br@SWCNTs complex was well dispersed in MeOH after QR (Fig. 4). It preliminarily indicated that the solubility of the PFPy-50@SWCNTs complex has been changed. There was no flocculation observed even after the PFPy-50-Br@SWCNTs complex stood for 48 h on the desktop (Fig. 3 inset). Also, it was used to detect directly UV-Vis-NIR spectroscopy (Fig. 5a). Comparison to those of raw SWCNTs, the characteristic peaks with metallic SWCNTs of the PFPy-50-Br@SWCNTs complex were not displayed in MeOH. However, there was also no obvious transition range that is similar to the PFPy-50@SWCNTs complex about S33 to 700 nm (the dotted line circles) on account of the tail absorption of polymer PFPy-50-Br after QR. The peaks of sc-SWCNTs at S22 appeared as a slight red shift (marked by *). To explore the reason of the red shift, the PFPy-50-Br@SWCNTs complex and PFPy-50-Br*@SWCNTs dispersions were compared in MeOH (ESI, Fig. S6†). Their sc-SWCNTs peaks completely overlapped at S22 after normalized at 939 nm. Generally, the SWCNTs-solvent interactions rose
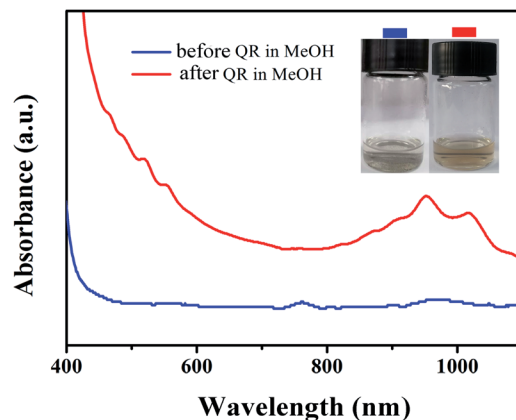

Fig. 4 UV-Vis-NIR spectra of PFPy-50@SWCNTs before QR (blue line) and after QR (red line) dispersed in MeOH. Physical picture before QR and after QR of PFPy-50@SWCNTs in MeOH.

from the induced dipole-induced dipole (Debye) interactions in polar solvents.[44,45] With the tractions of alcohol-soluble PFPy-50, the interactions between SWCNTs and MeOH become stronger. Therefore, the slight red shift may be caused by stronger Debye interactions at the SWCNTs–methanol interface.

To further investigate the nanotube characteristic before and after QR, Raman spectroscopy was performed at 785 nm, 633 nm and 532 nm excitation wavelengths, respectively. Fig. 5b shows the radial breathing modes (RBM) of laser at 785 nm excitation. Comparatively, the M11 characteristic absorption of raw SWCNTs presented a strong discrimination ability. The
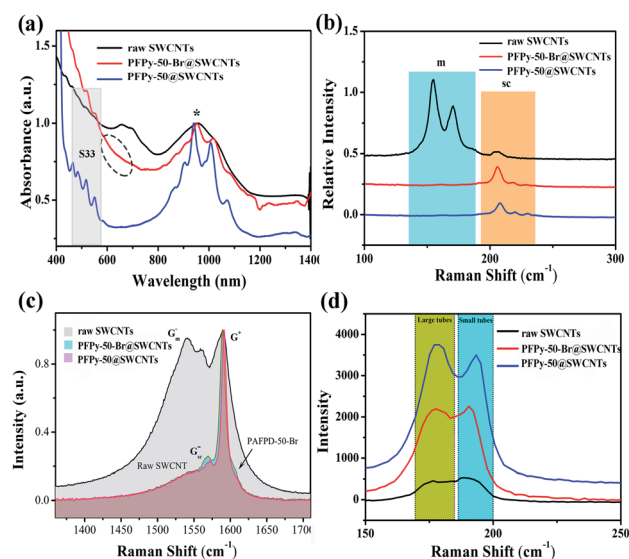

Fig. 5 (a) UV-Vis-NIR spectra of raw SWCNTs (black line), PFPy-50@SWCNTs (blue line) and PFPy-50-Br@SWCNTs dispersion (red line); (b) RBM spectra (100–300 cm^{-1}) of raw SWCNTs, PFPy-50@SWCNTs and PFPy-50-Br@SWCNTs dispersion at 785 nm; (c) Raman spectroscopy of G band ranges for raw SWCNTs, PFPy-50@SWCNTs and PFPy-50-Br@SWCNTs at 633 nm; (d) Raman spectrum of RBM mode raw SWCNTs, PFPy-50@SWCNTs and PFPy-50-Br@SWCNTs at 532 nm.
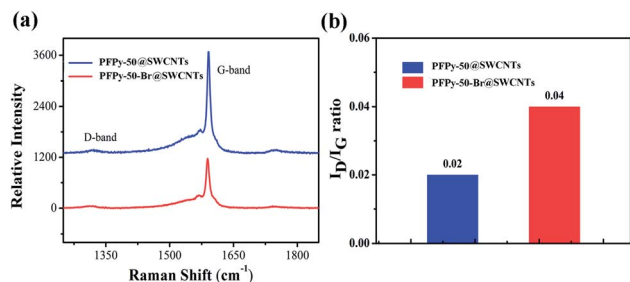
Fig. 6 (a) Raman spectra with D-mode and G-mode of PFPy-50@SWCNTs (blue line) and PFPy-50-Br@SWCNTs (red line) at 633 nm. (b) I_D/I_G ratio (integrated intensity ratio of the D-band and G-band) of PFPy-50@SWCNTs (blue box) and PFPy-50-Br@SWCNTs (red box).
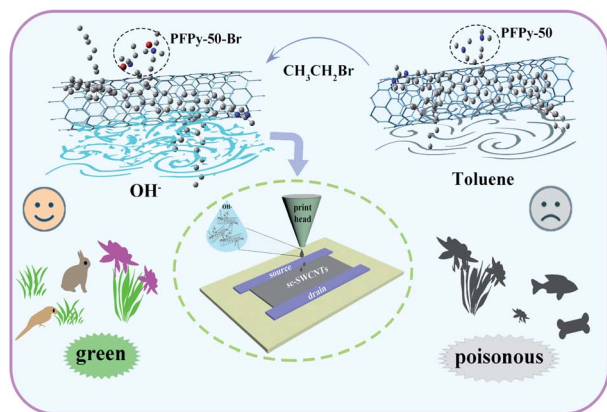

Fig. 7 SWCNTs dispersed in MeOH and TL solvents to influence the environment and industry. Dispersible SWCNTs are envisaged for the printing head in the alcohol system (inset).

Raman signals at the 633 nm excitation wavelength were obtained under the resonance excitation of M11 (Fig. 5c). Compared with before QR, the G_{sc}^- band became more obvious after QR (PFPy-50-Br@SWCNTs). Also, the emergence of the shoulder peak next to G^+ was caused by too much PFPy-50-Br. The frequencies of the Raman scattering (ω_{RBM}) on the size distributions of SWCNTs at the 532 nm excitation wavelength were inversely proportional to the diameters (dt) of SWCNTs, following the Kataura plot and the equation $\omega_{RBM} = A/dt + B$.[47] The sc-SWCNTs with diameters between 1.1 nm and 1.4 nm were obtained after QR, as shown in Fig. 5d.

Fig. 6a shows the D (1322 cm^{-1}) modes and G modes (1590 cm^{-1}). The increase in the D-band indicated an increase in the sp^3-hybridized carbon atoms on the SWCNTs sidewall. The integrated intensity ratio (I_D/I_G) of the D-band to the G-band was a parameter sensitive to the defect density (Fig. 6b). The I_D/I_G ratio of the sample from 0.02 increased to 0.04 after QR. From the total results, the I_D/I_G ratio still maintained the smallest value throughout the reaction, manifesting a little damage to the sidewalls during the functional reaction. Therefore, if the SWCNTs of high electronic performance are required in the

application, this method needs to be further optimized to obtain high-quality sc-SWCNTs.

As shown in Fig. 7, the conversion of SWCNTs from TL to MeOH solvents significantly reduces pollution in the surrounding and the human body. Also, methanol is cheaper and easier to obtain than toluene. Moreover, the alcohol solvent provides a possible reference in printing TFT processes for solving the print head's clogging problem because of its variety of ideal rheological properties (Fig. 7 inset).[31,48]

Conclusions

Based on the two characteristics, the tertiary amine groups can be functionalized into alcohol solubility and pyrimidine rings can select sc-SWCNTs. A route to functionalize and selectively separate alcohol-soluble sc-SWCNTs has been developed. Poly[(9,9-dioctylfluorene)-2,7-(9,9-bis(3′-(N,N-dimethylamino)propyl)-fluorene]$_{50}$-alt-[2-methylpyrimidine-2,7-(9,9-dioctylfluorene)]$_{50}$ is used to separate sc-SWCNTs with a purity greater than 99% via the reasonable adjustment of the polymer backbone. It has been investigated that diameters of alcohol-soluble sc-SWCNTs were mainly concentrated in 1.1–1.4 nm after the quaternization reaction, as investigated using UV-Vis-NIR spectroscopy and Raman scattering detection techniques. Also, the photoelectric properties of SWCNTs are still maintained. It is observed that the electron-rich conjugated system is beneficial to the selection of sc-SWCNTs, while the electron-poor frameworks are slightly inclined to choose m-SWCNTs by DFT calculation.

Conflicts of interest

There are no conflicts of interest to declare.

Acknowledgements

References

1 S. Iijima, Helical microtubules of graphitic carbon, *Nature*, 1991, **354**, 56–58.

2 T. Lei, L. L. Shao, Y. Q. Zheng, G. Pitner, G. Fang, C. Zhu, S. Li, R. Beausoleil, H.-S. P. Wong and T. C. Huang, Low-voltage high-performance flexible digital and analog circuits based on ultrahigh-purity semiconducting carbon nanotubes, *Nat. Commun.*, 2019, **10**, 1–10.

3 H. Chen, Y. Cao, J. Zhang and C. Zhou, Large-scale complementary macroelectronics using hybrid integration of carbon nanotubes and IGZO thin-film transistors, *Nat. Commun.*, 2014, **5**, 4097–4109.

4 P. M. Ajayan, Nanotubes from carbon, *Chem. Rev.*, 1999, **99**, 1787–1800.

5 Y. Cao; S. Cong; X. Cao; F. Wu; Q. Liu; M. R. Amer and C. Zhou, Review of electronics based on single-walled carbon nanotubes, *Topics in current chemistry*, 2017, vol. 375, pp. 189–224.

6 Q. Zhang, J. Q. Huang, W. Z. Qian, Y. Y. Zhang and F. Wei, The road for nanomaterials industry: a review of carbon nanotube production, post-treatment, and bulk applications for composites and energy storage, *Small*, 2013, **9**, 1237–1265.

7 S. M. Bachilo, M. S. Strano, C. Kittrell, R. H. Hauge, R. E. Smalley and R. B. Weisman, Structure-assigned optical spectra of single-walled carbon nanotubes, *Science*, 2002, **298**, 2361–2366.

8 M. Brohmann, F. J. Berger, M. Matthiesen, S. P. Schießl, S. Schneider and J. Zaumseil, Charge transport in mixed semiconducting carbon nanotube networks with tailored mixing ratios, *ACS Nano*, 2019, **13**, 7323–7332.

9 A. E. Islam, J. A. Rogers and M. A. Alam, Recent Progress in Obtaining Semiconducting Single-Walled Carbon Nanotubes for Transistor Applications, *Adv. Mater.*, 2015, **27**, 7908–7937.

10 J. Wang, T. D. Nguyen, Q. Cao, Y. Wang, M. Y. C. Tan and M. B. Chan-Park, Selective Surface Charge Sign Reversal on Metallic Carbon Nanotubes for Facile Ultrahigh Purity Nanotube Sorting, *ACS Nano*, 2016, **10**, 3222–3232.

11 K. S. Kim, G. Cota-Sanchez, C. T. Kingston, M. Imris, B. Simard and G. Soucy, Large-Scale Production of Single-Walled Carbon Nanotubes by Induction Thermal Plasma, *J. Phys. Appl. Phys.*, 2007, **40**, 2375–2387.

12 H. S. Lin, S. Okawa, Y. Ma, S. Yotsumoto, C. Lee, S. Tan, S. Manzhos, M. Yoshizawa, S. Chiashi, H. M. Lee, T. Tanaka, H. Kataura, I. Jeon, Y. Matsuo and S. Maruyama, Polyaromatic Nanotweezers on Semiconducting Carbon Nanotubes for the Growth and Interfacing of Lead Halide Perovskite Crystal Grains in Solar Cells, *Chem. Mater.*, 2020, **32**, 5125–5133.

13 S. Seo, I. Jeon, R. Xiang, C. Lee, H. Zhang, T. Tanaka, J. W. Lee, D. Suh, T. Ogamoto, R. Nishikubo, A. Saeki, S. Chiashi, J. Shiomi, H. Kataura, H. M. Lee, Y. Yang, Y. Matsuo and S. Maruyama, Semiconducting carbon nanotubes as crystal growth templates and grain bridges in perovskite solar cells, *J. Mater. Chem. A*, 2019, **7**, 12987–12992.

14 L. Huaping, T. Yifan, G. Wenmin, L. Hongyu, Zh. Lili and S. Nina, Polyfluorinated Electrolyte for Fully Printed Carbon Nanotube Electronics, *Adv. Funct. Mater.*, 2016, **26**, 6914–6920.

15 M. S. Arnold, A. A. Green, J. F. Hulvat, S. I. Stupp and M. C. Hersam, Sorting Carbon Nanotubes by Electronic Structure Using Density Differentiation, *Nat. Nanotechnol.*, 2006, **1**, 60–65.

16 M. Zheng, A. Jagota, E. D. Semke, B. A. Diner, R. S. McLean, S. R. Lustig, R. E. Richardson and N. G. Tassi, DNA-Assisted Dispersion and Separation of Carbon Nanotubes, *Nat. Mater.*, 2003, **2**, 338–342.

17 H. Liu, D. Nishide, T. Tanaka and H. Kataura, Large-Scale Single-Chirality Separation of Single-Wall Carbon Nanotubes by Simple Gel Chromatography, *Nat. Commun.*, 2011, **2**, 309.

18 M. Engel, J. P. Small, M. Steiner, M. Freitag, A. A. Green, M. C. Hersam and P. Avouris, Thin Film Nanotube Transistors Based on Self-Assembled, Aligned, Semiconducting Carbon Nanotube Arrays, *ACS Nano*, 2008, **2**, 2445–2452.

19 A. Nish, J. Y. Hwang, J. Doig and R. J. Nicholas, Highly Selective Dispersion of Single-Walled Carbon Nanotubes using aromatic polymers, *Nat. Nanotechnol.*, 2007, **10**, 640–646.

20 L. Ting, Ch. Xiyuan, P. Gregory, H.-S. Philip W. and Z. Bao., Removable and Recyclable Conjugated Polymers for Highly Selective and High-Yield Dispersion and Release of Low-Cost Carbon Nanotubes, *J. Am. Chem. Soc.*, 2016, **138**, 802–805.

21 K. Catherine, J. B. Gerald, J. S. Matthew, H. Peishen, J. Yongho, S. A. Michael and G. Padma, Structurally Analogous Degradable Version of Fluorene-Bipyridine Copolymer with Exceptional Selectivity for Large-Diameter Semiconducting Carbon Nanotubes, *ACS Appl. Mater. Interfaces*, 2017, **9**, 40734–40742.

22 J. Yongho, J. B. Gerald, J. S. Matthew, O. M. Belésn, K. Catherine, K. S. Samantha, M. W. Bryan, S. A. Michael and G. Padma, Isolation of Pristine Electronics Grade Semiconducting Carbon Nanotubes by Switching the Rigidity of the Wrapping Polymer Backbone on Demand, *ACS Nano*, 2015, **9**, 10203–10213.

23 X. Wei and X. Maimaitiyiming, Selectable and Releasable Noncovalent Functionalization of Semiconducting SWCNTs by Biethynyl- 2, 5- bis (dodecoxy) benzene Unit-Containing Conjugated Copolymers, *Macromol. Chem. Phys.*, 2020, 2000086–2000093.

24 T. Lei, I. Pochorovski and Z. Bao, Separation of Semiconducting Carbon Nanotubes for Flexible and Stretchable Electronics Using Polymer Removable Method, *Acc. Chem. Res.*, 2017, **50**, 1096–1104.

25 W. Huiliang, H. Bing, O. Gonzalo Jiménez, L. Peng, J. T. Christopher, D. Ying, L. Ting, N. H. Kendall and B. Zhenan, Solvent Effects on Polymer Sorting of Carbon Nanotubes with Applications in Printed Electronics, *Small*, 2015, **11**, 126–133.

26 Q. Song, W. Kunjie, G. Bing, L. Liqiang, J. Hehua and L. Qingwen, Solution-Processing of High-Purity Semiconducting Single-Walled Carbon Nanotubes for Electronics Devices, *Adv. Mater.*, 2019, **31**, 1800750–1800771.

27 G. Wei, X. Wenya, Y. Jun, L. Tingting, W. Junkai, T. Hongwei, L. Yi, T. Masayoshi, S. Dongfeng, W. Liangzhuan, O. Toshiya and Y. Yingjun, Selective Dispersion of Large-Diameter Semiconducting Carbon Nanotubes by Functionalized Conjugated Dendritic Oligothiophenes for Use in Printed Thin Film Transistors, *Adv. Funct. Mater.*, 2017, **27**, 1703938–1703948.

28 X. Wei and X. Maimaitiyiming, Enrichment of highly pure large-diameter semiconducting SWCNTs by polyfluorene-containing pyrimidine ring, *RSC Adv.*, 2019, **9**, 32753–32758.

29 A. Kojiro, T. Fumiyuki, O. Hiroaki, F. Tsuyohiko and N. Naotoshi, Recognition and One-Pot Extraction of Right- and Left-Handed Semiconducting Single-Walled Carbon Nanotube Enantiomers Using Fluorene-Binaphthol Chiral Copolymers, *J. Am. Chem. Soc.*, 2012, **134**, 12700–12707.

30 Y. Sweejiang, Y. Wenhui, K. Asif, S. Jinhai and H. Xun, Separation of Large-Diameter Metallic and Semiconducting Single-Walled Carbon Nanotubes by Iterative Temperature-Assisted Gel-Column Chromatography for Enhanced Device Applications, *Phys. Status Solidi B*, 2020, **257**, 1900714–1900721.

31 J. Y. Ouyang, J. F. Ding, J. Lefebvre and P. R. L. Malenfant, Sorting of Semiconducting Single-Walled Carbon Nanotubes in Polar Solvents with an Amphiphilic Conjugated Polymer Provides General Guidelines for Enrichment, *ACS Nano*, 2018, **12**, 1910–1919.

32 D. Fong, G. M. Andrews, S. A. Mcnelles and A. Adronov, Decoration of polyfluorene-wrapped carbon nanotube thin films *via* strain-promoted azide–alkyne cycloaddition, *Macromolecules*, 2018, **51**, 755–768.

33 F. Darryl, Y. Jason, M. Eric and A. Alex, Reactive, Aqueous-Dispersible Polyfluorene-Wrapped Carbon Nanotubes Modulated with an Acidochromic Switch *via* Azide-Alkyne Cycloaddition, *ACS Appl. Polym. Mater.*, 2019, **1**, 797–803.

34 J. Y. Ouyang, J. F. Ding, J. Lefebvre and P. R. L. Malenfant, Sorting of Semiconducting Single-Walled Carbon Nanotubes in Polar Solvents with an Amphiphilic Conjugated Polymer Provides General Guidelines for Enrichment, *ACS Nano*, 2018, **12**, 1910–1919.

35 Y. Maimaiti and X. Maimaitiyiming, Fluorescence quenching of methanol-soluble polypyrimidine by aluminum ion, *Mater. Express*, 2020, **7**, 1177–1188.

36 D. Fong and A. Adronov, Investigation of Hybrid Conjugated@Nonconjugated Polymers for Sorting of Single-Walled Carbon Nanotubes, *Macromolecules*, 2017, **50**, 8002–8009.

37 T. Lei, Y. C. Lai, G. Hong and Z. H. N. Bao, Diketopyrrolopyrrole (DPP)-Based Donor-Acceptor Polymers for Selective Dispersion of Large-Diameter Semiconducting Carbon Nanotubes, *Small*, 2015, **11**, 2946–2954.

38 T. Lei, J. Y. Wang and J. Pei, Design, Synthesis, and Structure-Property Relationships of Isoindigo-Based Conjugated Polymers, *Acc. Chem. Res.*, 2014, **4**, 1117–1126.

39 H. Zhang, X. Zhao, J. Bai, Y. Hou, Sh. Wang, Ch. Wang and D. Ma, Ternary Memory Devices Based on Bipolar Copolymers with Naphthalene Benzimidazole Acceptors and Fluorene/Carbazole Donors, *Macromolecules*, 2019, **52**, 9364–9375.

40 R. Kang, S. H. Oh and D. Y. Kim, Influence of the ionic functionalities of Polyfluorene derivatives as a cathode interfacial layer on inverted polymer solar cells, *ACS Appl. Mater. Interfaces*, 2014, **9**, 6227–6236.

41 J. Kim, D. Khim, R. Kang, S. H. Lee, K. J. Baeg, M. Kang, Y. Y. Noh and D. Y. Kim, Simultaneous Enhancement of Electron Injection and Air Stability in N-Type Organic Field-Effect Transistors by Water-Soluble Polyfluorene Interlayers, *ACS Appl. Mater. Interfaces*, 2014, **11**, 8108–8114.

42 H. Ozawa, T. Fujigaya, Y. Niidome, N. Hotta and M. Fujiki, Naotoshi NakashimaRational Concept To Recognize/ Extract Single-Walled Carbon Nanotubes with a Specific Chirality, *J. Am. Chem. Soc.*, 2011, **133**, 2651–2657.

43 S. Chiashi, K. Kono, D. Matsumoto, J. Shitaba, N. Homma, A. Beniya, T. Yamamoto and Y. Homma, Adsorption Effects on Radial Breathing Mode of Single-Walled Carbon Nanotubes, *Phys. Rev. B: Condens. Matter Mater. Phys.*, 2015, **91**, 155415.

44 D. Fong, W. J. Bodnaryk, N. A. Rice, S. Saem, J. M. Moran-Mirabal and A. Adronov, Influence of Polymer Electronics on Selective Dispersion of Single-Walled Carbon Nanotubes, *Chem. - Eur. J.*, 2016, **22**, 14560–14566.

45 Z. Zhou, M. Steigerwald, M. Hybertsen, L. Brus and R. A. Friesner, High-efficiency, environment-friendly electroluminescent polymers with stable high work function metal as a cathode: Green-and yellow-emitting conjugated polyfluorene polyelectrolytes and their neutral precursors, *J. Am. Chem. Soc.*, 2004, **126**, 3597–3607.

46 B. A. Larsen, P. Deria, J. M. Holt, I. N. Stanton, M. J. Heben, M. J. Therien and J. L. Blackburn, Effect of Solvent Polarity and Electrophilicity on Quantum Yields and Solvatochromic Shifts of Single-Walled Carbon Nanotube Photoluminescence, *J. Am. Chem. Soc.*, 2012, **134**, 12485–12491.

47 F. Yang, M. Wang, D. Zhang, J. Yang, M. Zheng and Y. Li, Chirality Pure Carbon Nanotubes: Growth, Sorting, and Characterization, *Chem. Rev.*, 2020, **120**, 2693–2758.

48 H. Wang, B. Hsieh, G. Jiménez-Osés, P. liu, C. J. Tassone, Y. Diao, T. Lei, K. N. Houk and Z. Bao, Solvent effects on polymer sorting of carbon nanotubes with applications in printed electronics, *Small*, 2015, **11**, 126–133.